Discrete tones generated by the impingement of a high-speed jet on a circular cylinder

AUTHOR(S):

UMEDA, Yoshikuni; MAEDA, Hiroshi; ISHII, Ryuji

Discrete tones generated by the impingement of a high-speed jet on a circular cylinder

By

Yoshikuni UMEDA*, Hiroshi MAEDA* and Ryuji ISHII*

(Received December 23, 1986)

Abstract

Experimental measurements were made of the frequencies of discrete tones emanating from high subsonic and choked underexpanded jets of air issuing from a circular nozzle and impinging on a slender circular cylinder placed normal to the jet axis. In the experiments, a few types of discrete tones were observed. It is proved that the frequencies of the discrete tones can be calculated by using a feedback model proposed by Powell, and Ho and Nosseir.

Schlieren photographs of the flowfield along with the near-sound field were taken for various nozzle-to-cylinder distances and various pressure ratios. Close investigation of these schlieren photographs has shown that for the subsonic jet, one strong sound wave is emitted near the cylinder and two large ring vortices are produced near the nozzle exit during one cycle of the feedback loop. These two large ring vortices merge together in a later stage of the loop. For the choked underexpanded jet, one strong sound wave is emitted and one large ring vortex is produced during one cycle of the feedback loop. In this case, a merging of the successive large ring vortices has not occurred.

1. Introduction

Recently, Ho and Nosseir[1] performed a detailed study of sounds emitted from an axisymmetric high subsonic jet impinging on a flat plate placed normal to the jet axis. Their measurements have clearly shown a strong resonance in the flow caused by the forcing of the unstable shear layers by an upstream-propagating periodic pressure field through the ambient region of the jet. The propagating pressure field was associated with the impingement of coherent flow structures on the plate. The pressure disturbance was seen to interact with the shear layer instability to form coherent structures which convect downstream to close a feedback loop. A similar phenomenon was also observed by Wagner[2] and Marsh.[3] Krothapalli[4] conducted a similar experiment by using an under-expanded rectangular jet, and found that a screech tone was radiated in addition

* Department of Aeronautical Engineering, Kyoto University, Kyoto, Japan.

to the impinging tone.

In our experiment, a new configuration of discrete tone was found. This discrete tone is radiated when a circular cylinder is placed in high subsonic and choked underexpanded jets normal to the jet axis near the nozzle exit. The principal parameters characterizing the frequency of the discrete tone are the flow Mach number M or the pressure ratio R (stagnation pressure / ambient pressure) of the jet, the nozzle diameter d, and the nozzle-to-cylinder distance x. In the present paper, the flow Mach number M is related with the pressure ratio R through a fully expanded isentropic flow.

In order to investigate the generation mechanism of the present discrete tone, the following experiments were carried out:

(1) The spectrum and overall sound pressure level of sounds emitted from a jet were measured for various pressure ratios, locations of the cylinder and the nozzle diameters.

(2) Schlieren photographs of the jet were taken in order to visualize the flowfield along with the near-sound field.

From these experiments, it will be shown that the frequency characteristics of the present discrete tone radiated from a high subsonic jet are clearly different in some respects from those of the other types of discrete tones investigated previously.

For the choked underexpanded jet, a stabilization phenomenon of the jet by placing a circular cylinder was found for some particular pressure ratio and nozzle-to-cylinder distance. In the stabilized jet, the asymmetric mode of instability is suppressed and the cellular structure is enhanced. In this case, the helical mode of screech tone which is usually radiated from a free jet was not observed.

2. Experimental Apparatus

A detailed description of the experimental apparatus was presented in the previous paper.[5] In the present paper, however, a few important improvements were made. The measurements of sound pressure were made by using a 0.32-cm-diameter Bruel and Kjaer type-4135 condenser microphone, which has a flat response out to about 100 kHz. The microphone was located at a fixed position in the backward arc about 50 degrees from the jet axis, at a radius of 1.35 m from the nozzle exit, and 1.50 m above the floor. All the signal outputs were recorded on a TEAC-R-410 data recorder. The direct mode recording was made

for the frequency band from 100 Hz to 100 kHz. The experiments for the frequency characteristics of the discrete tones were carried out on the following conditions:

(1) The Mach number M or the pressure ratio R ($=P_0/P$, where P_0 is the stagnation pressure and P is the ambient pressure) of the jet is fixed, and the nozzle-to-cylinder distance x is changed.

(2) The nozzle-to-cylinder distance x is fixed, and the flow Mach number M or the pressure ratio R of the jet is changed.

The analogue data were digitized by a Fujitsu U-200 minicomputer and processed on a Fujitsu M-200 computer in the Data Processing Center of Kyoto University. The fast Fourier transform (FFT) method was used for all the spectral analysis, and the spectral curves were drawn by an X-Y plotter.

For the flow visualization, the optics employed was a conventional schlieren setup, which was a single-pass design with the optical axis folded twice by using two spherical mirrors (diameter of 20 cm and focal length of 200 cm). In the present experiment, two types of light sources were employed. For long-time-exposure (1/30 sec) schlieren photographs, a mercury discharge lamp which illuminates continuously was employed. For instantaneous schlieren photographs, the light source employed was a stroboscopic flash unit having flash durations adjustable at 1.1 – 4.5 μs at four discrete settings. We always set the flash duration at 1.1 μs to take the instantaneous schlieren photographs.

The controlling parameter for the jet was the stagnation pressure P_0, which varied at 1.0 – 6.0 kg/cm^2. The nozzle-to-cylinder distance x was varied discretely at 0.5 – 10.0 cm.

3. Frequency Characteristics

At a high Reynolds number, turbulent mixing commencing at the shear layers of jet boundaries is responsible for the jet-noise with a continuous frequency spectrum. In general, the jet is highly unstable at a high Reynolds number, and in some situations both discrete and broadband components are radiated from the jet. The present study focuses on the discrete components alone.

Typical spectra of sounds emitted from high subsonic and choked underexpanded jets are shown in Figs. 1 and 2, respectively. In these figures, the abscissa is the sound frequency and the ordinate is the sound pressure level in decibels. The spectrum in Fig. 1 a is for a subsonic free jet, and the spectrum in

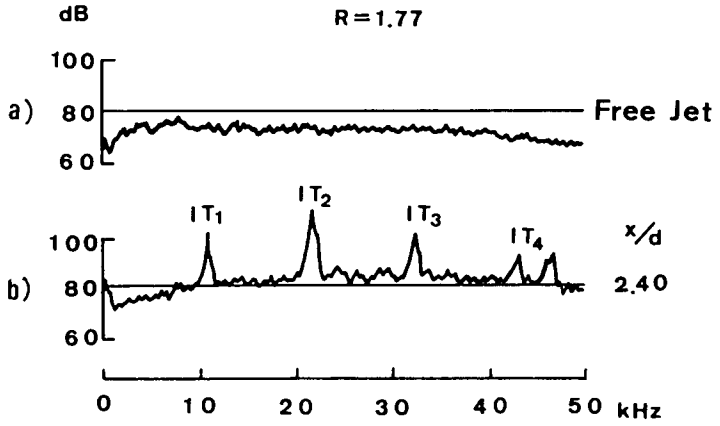

Fig. 1 Spectra of sounds emitted from high subsonic jet: a) jet noise for $R=1.77$, b) discrete tone for $R=1.77$ and $x/d=2.40$.

Fig. 1 b is for the same jet where the cylinder is placed at $x/d=2.40$ ($d=1.00$ cm). In the latter spectrum, several sharp peaks are seen in addition to the ordinary jet noise. These are the frequencies of the discrete tones. The spectrum in Fig. 2 a is for a supersonic free jet, and the spectra in Figs. 2 b to 2 g are for the same choked underexpanded jet in which a cylinder is placed. Although the characteristics of the resonance phenomenon for a choked jet are essentially the same as those for the high subsonic jet, one different kind of discrete tone is radiated from the choked jet. This is the so-called screech tone whose wavelength is related to the regular shock wave spacing. Since the screech tone is radiated only from a choked underexpanded supersonic jet and its wavelength does not appreciably depend on the presence of the cylinder, it can be identified in the observed spectrum by making use of such characteristics.

In order to avoid confusion, in what follows, we use the term "impinging tone" after Krothapalli[4] for the discrete tone which is radiated from a jet only when a cylinder is placed in it. This is because this discrete tone is radiated due to a feedback loop consisting of the downstream-convecting vortex rings and the upstream-propagating sound waves outside (and inside, in the subsonic case,) the jet. In the present paper, therefore, the screech tone is distinguished from the "impinging tone". In Figs. 1 and 2, the impinging tone and the screech tone are denoted by the symbols IT_n and SS_n, respectively, where $n=1, 2, 3, \cdots$. The subscript $n=1$ denotes the fundamental frequency and $n\geq 2$ denotes the higher harmonics.

In Figs. 3 a to 3 c, the resonance frequencies f of the impinging tones were plotted against the nozzle-to-cylinder distance x/d for $R=1.77$, 2.45, and 3.90. In

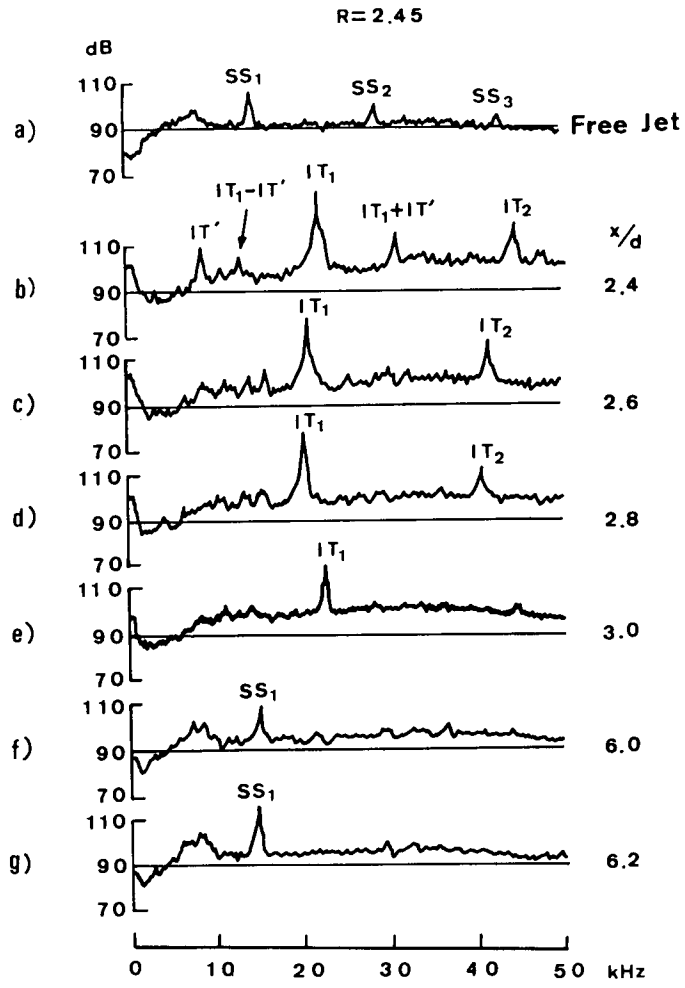

Fig. 2 Spectra of sounds emitted from choked underexpanded jet: a) free jet for $R=$ 2.45, b) -g) jet with cylinder for $R=2.45$ and $x/d=2.4$, 2.6, 2.8, 3.0, 6.0, and 6.2.

Figs. 4 a and 4 b, the resonance frequencies f of the impinging tones were plotted against the pressure ratio R for $x/d=2.40$ and 3.00 ($d=1.00$ cm). In these figures, the black circles represent the frequencies of the impinging tones with prominent peaks whose sound pressure levels exceed those of the broad frequency band by 10 dB or more. The white circles represent the frequencies of sounds with small peaks whose sound pressure levels exceed those of the broad frequency band by 5 - 10 dB.

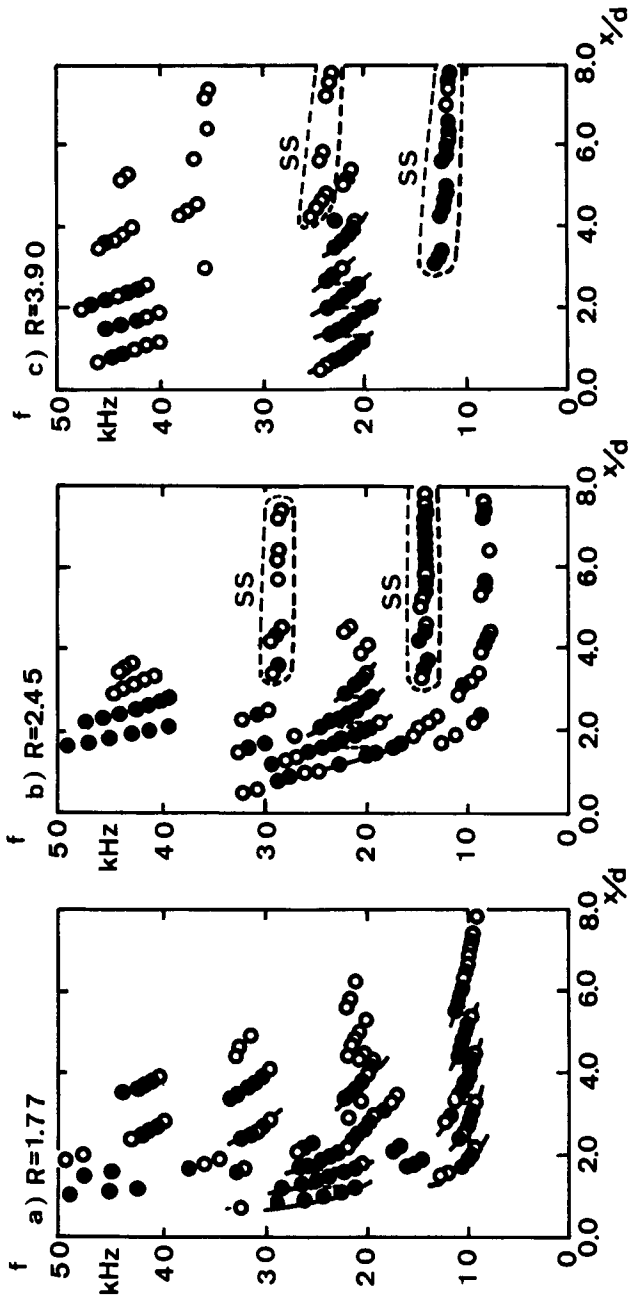

Fig. 3 Resonance frequency vs. nozzle-to-cylinder distance for fixed pressure ratio: a) $R = 1.77$, b) $R = 2.45$, c) $R = 3.90$.

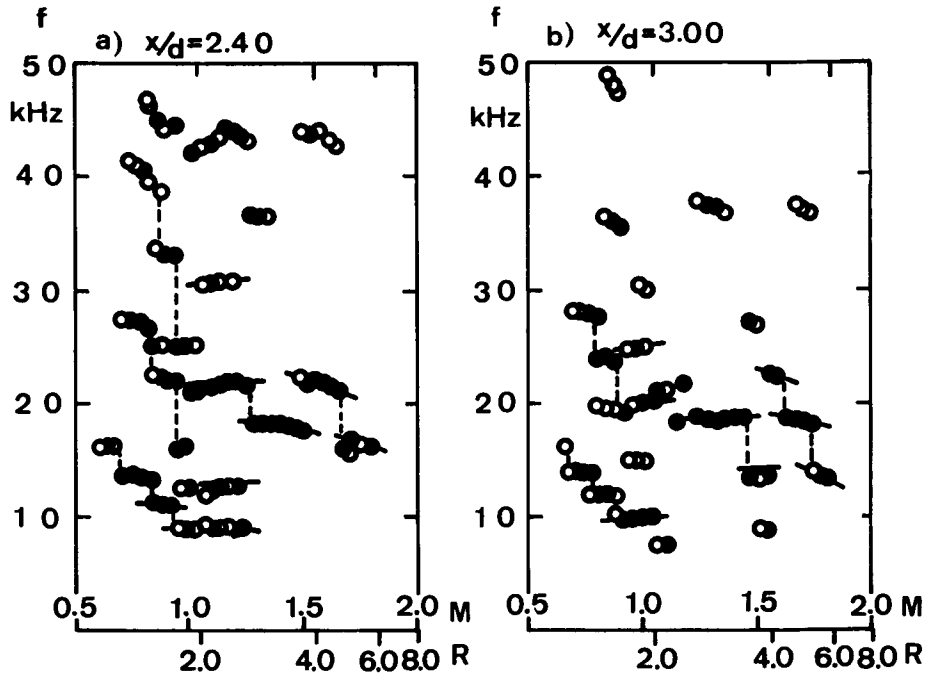

Fig. 4 Resonance frequency vs. pressure ratio for fixed nozzle-to-cylinder distance: a) $x/d = 2.40$. b) $x/d = 3.00$.

From the experimental results shown in Figs. 3 and 4, it is found that the impinging tone has the following characteristics:

(1) This tone is generated when the nozzle-to-cylinder distance x/d is in the range $0.5 - 8.0$ and a jet is operated at $M > 0.6$ ($R > 1.28$).

(2) When the Mach number M or the pressure ratio R of a jet is fixed, the resonance frequency of the impinging tone decreases gradually as the nozzle-to-cylinder distance is increased. The resonance frequency decreases until a certain nozzle-to-cylinder distance is reached. A further increase in the nozzle-to-cylinder distance results in a frequency jump to a higher mode of oscillation. Several modes of oscillations are demonstrated in Figs. 3a to 3c.

(3) As the pressure ratio R is increased for a fixed nozzle-to-cylinder distance x/d, the resonance frequency decreases stepwise as shown in Figs. 4a and 4b. For the range of the pressure ratio $2.0 < R < 2.3$, however, the resonance frequency shows an irregular change.

(4) A few harmonics are radiated in the frequency range below 50 kHz.

From these observations, it can be said that the frequency characteristics of

the impinging tone are somewhat different from those of the other types of discrete tones previously investigated. When the nozzle-to-cylinder distance is changed at a fixed pressure ratio, the frequency characteristics of the present discrete tone are similar to those of the edge tones and of the discrete tones radiated from a high subsonic jet impinging on a flat plate. However, when the pressure ratio is changed for a fixed nozzle-to-cylinder distance, the frequency characteristics of this discrete tone are different from the other types of discrete tones whose frequencies increase and jump to higher frequencies as the pressure ratio increases. Only the paper by Krothapalli[4] reported a similar behaviour of the resonance frequency. That is, for the fixed nozzle-to-plate distance in a supersonic jet, the resonance frequency decreases with the pressure ratio.

In Figs. 3 b and 3 c, two groups of circles surrounded by dotted lines *SS* show the screech tones. The frequencies of the screech tone are kept almost constant with respect to the nozzle-to-cylinder distance, as shown in Figs. 3 b and 3 c. It must be emphasized that, in our experiment, the screech tones are not observed when the cylinder is placed in the range of $x/d < 3$.

Frequencies of the screech tones radiated from a choked free jet are shown in Fig. 5 a for various pressure ratios. Figure 5 b shows the frequencies of

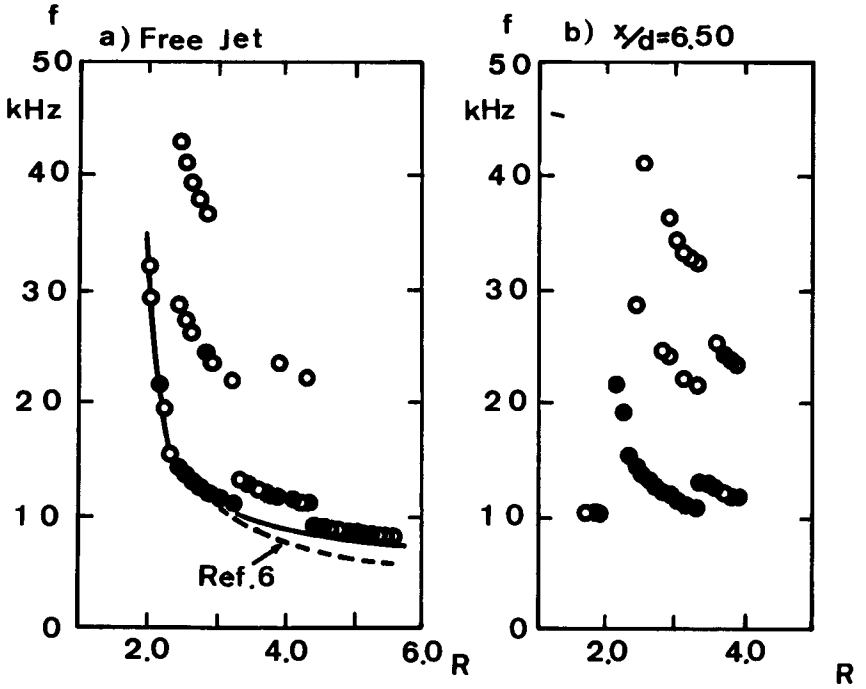

Fig. 5 Frequency of discrete tone vs. pressure ratio: a) screech tone, b) jet with cylinder for $x/d = 6.50$.

discrete tones radiated from a jet with the cylinder at $x/d = 6.50$. Comparing Figs. 5 a and 5 b, we can see that all the frequencies of the discrete tones shown in Fig. 5 b in the supersonic range ($R > 2$) agree with those in Fig. 5 a. These, then, are obviously the screech tones. This means that in the present experiment, the impinging tones are not radiated, but only the screech tones are observed from the choked jet for $x/d > 6.0$. Such a situation is also well demonstrated in Fig. 2.

4. Visualization of Jet Flows

In order to investigate the generation mechanism of the present impinging tone, a visualization of the flowfield along with the near-sound field was carried out by the schlieren method. In the present visualization, both instantaneous and long-time-exposure schlieren photographs were taken for various flow conditions. Both types of photographs were taken for various nozzle-to-cylinder distances x/d and pressure ratios R. In order to see the 3-dimensional structure of the flowfield, side view and top view photographs of the jet were taken by using a straight cylinder and a Γ-shaped cylinder, as shown in Figs. 6 a and 6 b.

Figures 7 and 8 show schlieren photographs of the jets for $R = 1.77$ ($M = 0.94$) and $x/d = 2.40$ and for $R = 2.45$ and $x/d = 2.40$, respectively, where a and b are the top views and c and d are the side views of the jet, respectively. The photographs in Figs. 7 b, 7 d, 8 b, and 8 d are the long-time-exposure ones, while those in Figs. 7 a, 7 c, 8 a, and 8 c are the instantaneous ones. Although

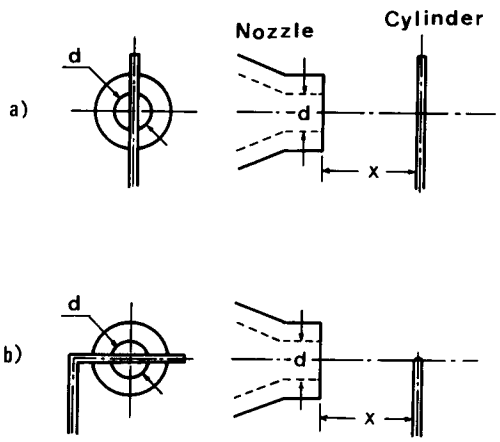

Fig. 6 Setting of cylinders for schlieren photographs: a) side view, b) top view.

all four photographs in Figs. 7 and 8 are, respectively, for the same jet, the corresponding long-time-exposure and instantaneous photographs seem to show completely different phenomena. In the long-time-exposure photographs of the subsonic jet, one can see some complicated fringe patterns in the jet almost normal to the jet axis (Figs. 7 b and 7 d) and a V-shaped wake behind the cylinder (Fig. 7 b). Especially for the fringe pattern, it is almost impossible to find its counterpart in the corresponding instantaneous photographs. The fringe pattern and wake in the long-time-exposure photographs did not change their shapes or locations even when the exposure time was changed from 1/1000 to 1/4 sec. However, the fringe pattern depended on the pressure ratio R and the nozzle-to-cylinder distance x/d. Various kinds of fringe patterns were observed for various combinations of R and x/d. Wagner[2] observed the same kind of fringe patterns when a subsonic jet was impinged on a flat plate placed normal to the jet axis. He explained these fringe patterns in the long-time-exposure photographs as standing sound waves in the jet. In our experiment, unfortunately, we could not prove this fact, at least for the present.

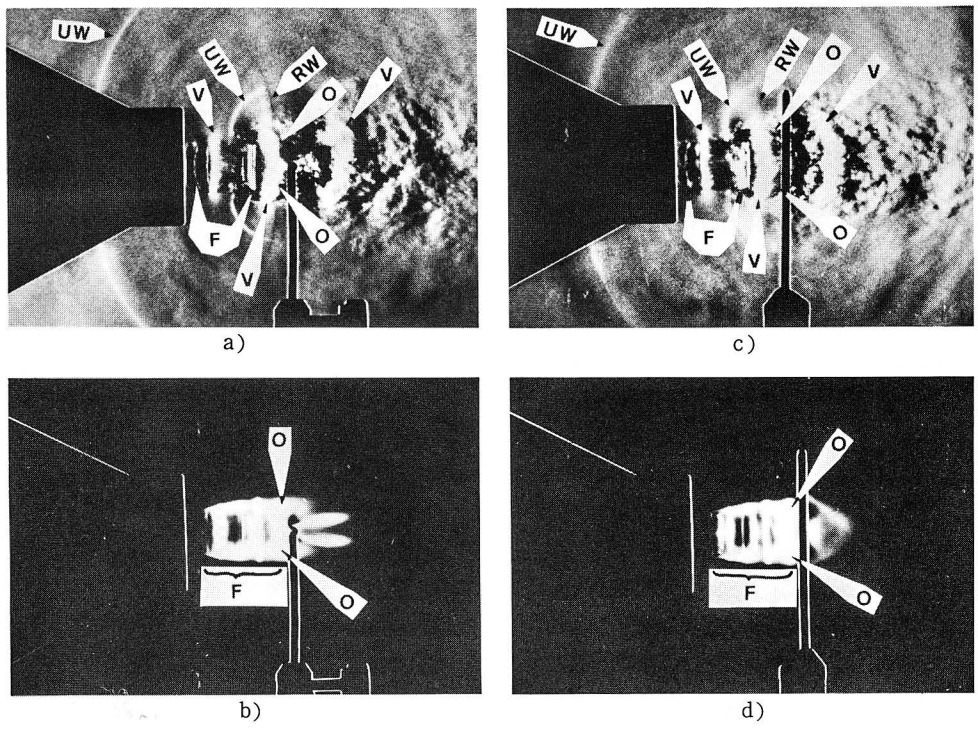

Fig. 7 Instantaneous and long-time-exposure schlieren photographs for $R=1.77$ and $x/d=2.40$: a) and b) top views, c) and d) side views.

In Figs. 7 a, 7 c, 8 a, and 8 c, one can see very clear and sharp white spherical sound wavefronts outside the jet, widely spreading ring vorticies surrounding the jet, and clear wavefronts or cellular structures inside the jet. In these figures, *UW*, *RW*, *V*, *F*, and *O* denote the upstream-propagating sound wave outside the jet, the downstream-propagating sound wave reflected from the nozzle-exit wall, the large ring vortex, the fringe pattern inside the jet, and the location of the apparent sound source, respectively. It is important to notice that no appreciable difference can be found between the shapes of the sound waves and those of the large ring vortices in Figs. 7 a and 7 c, and Figs. 8 a and 8 c, respectively. This means that the strong wavefront and the large ring vortex can be approximated to be axially symmetric. The sound sources denoted by *O* in these figures are merely the approximate geometrical centers of the waves propagating outside the jet. Since the strong sound is emitted near the cylinder in the jet, and then its wavefront would be distorted in the flowfield of the jet before it propagates outside the jet, it is reasonable to consider that the true sound source might be located at a little different point from the point *O*. The

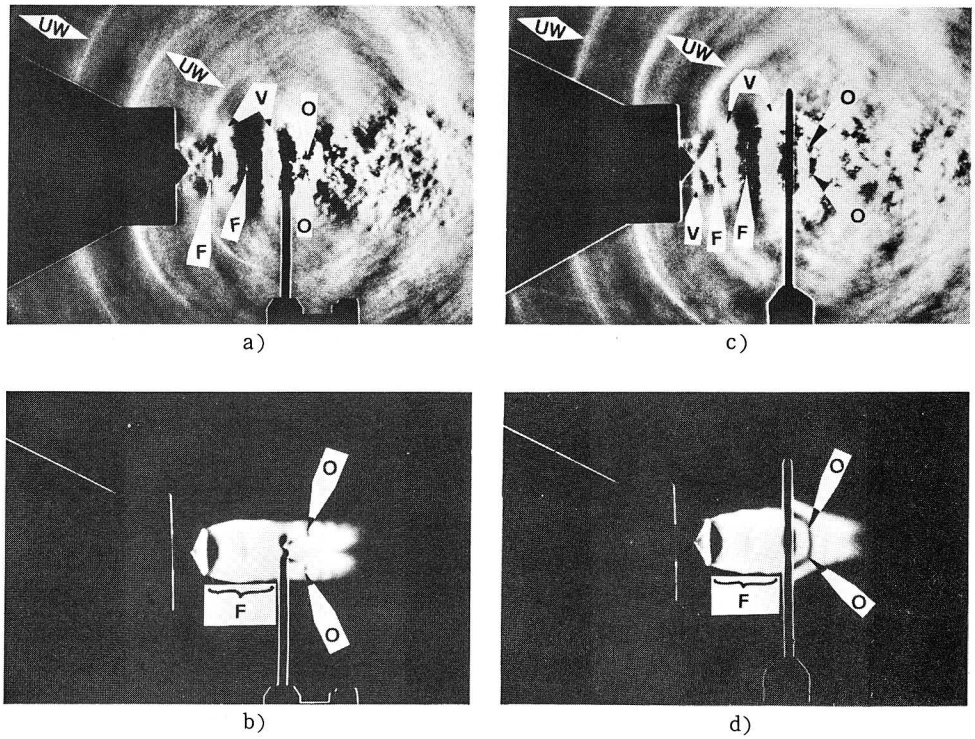

Fig. 8 Instantaneous and long-time-exposure schlieren photographs for supersonic jet for $R=2.45$ and $x/d=2.40$: a) and b) top views, c) and d) side views.

wavefronts of the strong sounds UW propagate at an angle of about 135 degrees to the direction of the jet stream. From these photographs, the wavelength of the sound (the distance between two successive wavefronts) and the approximate location of the sound source can be determined. With these results, in the next section, we will investigate the frequency characteristics of the impinging tone by making use of the idea proposed by Ho and Nosseir.[1]

5. Impinging Tone

Here, it is assumed that the impinging tone is radiated by a mechanism similar to the one proposed by Ho and Nosseir.[1] According to them, the impinging tone is generated by a feedback loop which consisted of the downstream-convected coherent structure (the periodic ring vortex) and the upstream -propagating pressure wave (the sound wave) generated by the traversing of the coherent structure through the cylinder. The velocity of the upstream-propagating pressure wave is the velocity of sound of the ambient region c_0. The velocity of the downstream-convected ring vortex is about 0.62 times the jet exhaust speed U (Ho and Nosseir[1]). Here, it is considered that the jet exhausted speed U is given by the flow velocity based on a fully expanded isentropic flow. This is given by

$$U=c_0 M/\sqrt{1+M^2/5} \tag{1}$$

where

$$M=\sqrt{5\,(R^{2/7}-1)} \tag{2}$$

Then we have

$$v=0.62\,U=0.62\,c_0 M/\sqrt{1+M^2/5}=c_0/A \quad \text{(for air)} \tag{3}$$

where, $A=\sqrt{1+M^2/5}\,/0.62\,M$. Therefore, if we assume that the sound sources are located on the rear edge of the first cellular structure, the time interval T for a feedback loop to close is given by

$$T=l/c_0+l/v=l(1+A)/c_0 \tag{4}$$

where l is the distance from the nozzle exit to the sound sources. The frequency of the impinging tone is given by

$$f=n/T=nc_0/(l(1+A)) = (n/K(1+A))\,(c_0/d) \qquad (n=1,\ 2,\ 3,\ \ldots\ldots) \qquad (5)$$

where $K=l/d$.

For the calculation of the frequency of this impinging tone, it is necessary to know the location of the sound source from the instantaneous schlieren photographs. Assuming that the upstream-propagating wavefront outside the jet is a spherical wave, the apparent sound source can roughly be approximated by the geometrical center of the spherical wave. The estimated locations of the sound sources O were marked on the photographs by arrowheads in Figs. 7 and 8 for the subsonic and supersonic jets, respectively. It is found from the instantaneous photographs for $R=1.77$ ($M=0.94$) and $x/d=2.40$, shown in Figs. 7a and 7c, that the approximate sound sources determined in such a manner exist at points a little upstream from the cylinder. These points correspond to the locations of the fringe patterns before the cylinder in the corresponding long-time-exposure photographs, as shown in Figs. 7b and 7d.

For the supersonic jet, the locations of sound sources nearly coincide with the intersections of the wake of the cylinder and the first end of the jet roll-up (Figs. 8a and 8c). These locations are also shown by arrowheads in the corresponding long-time-exposure photographs (Figs. 8b and 8d). With these locations of sound sources, we can determine the distances l from the nozzle exit to the sound sources, and then calculate the frequency of the impinging tones. In Fig. 9, the distances l are shown for the supersonic jet. The calculated frequencies by using Eq. (5) are shown in Figs. 3 and 4 by solid lines, and are compared with the microphone measurements. The agreement between them is very good.

From these considerations, we can conclude that the impinging tone (different from the screech tone) is radiated from high subsonic and choked underexpanded jets impinging on the slender circular cylinder placed normal to the jet axis by a similar mechanism as that proposed by Ho and Nosseir.[1]

In what follows, we will use a flow visualization technique in order to investigate the generation mechanism of the impinging tone. Figures 10a and 10b show instantaneous photographs of a subsonic jet taken at different instants. These are the photographs where the locations of the upstream-propagating

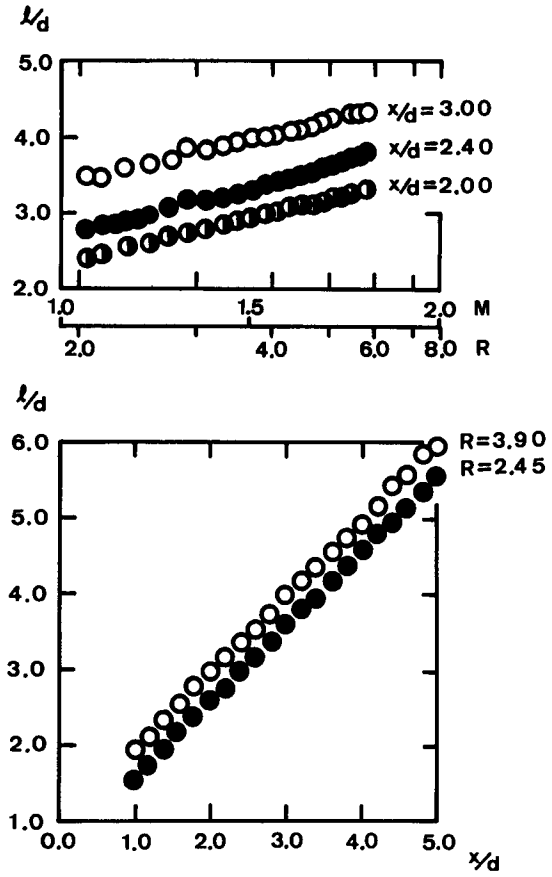

Fig. 9 Distance between sound source and nozzle exit.

wavefronts almost coincide with each other. Although these photographs were taken at a very long time interval, compared with a unit period for the generation of the discrete tone, the locations, sizes and shapes of the large ring vortices and the sound wave inside the jet in both photographs almost coincide with each other. As can be seen, these photographs are different only in minor and trivial scales of flow structures. Such a situation may strongly suggest that the predominant, large scale phenomena are repeated almost completely synchronously. Therefore, we can use the location of the upstream-propagating wavefront outside the jet as a reference time in order to investigate the mechanism of the feedback loop of the impinging tone.

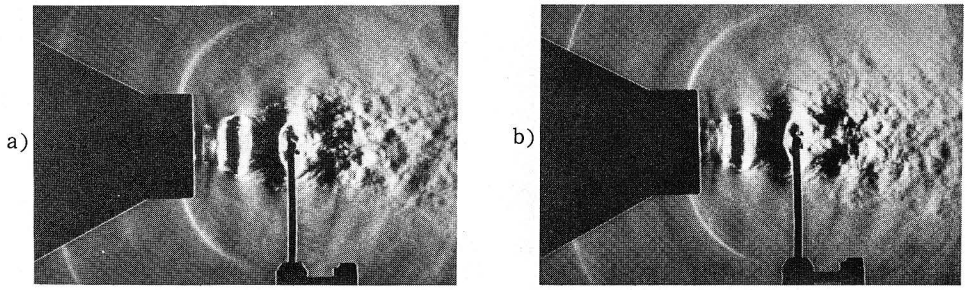

Fig. 10 Reproducibility of feedback phenomenon.

A. Subsonic jet

Figures 11 a to 11 l show a series of instantaneous photographs during one cycle of the impinging tone generation for $x/d = 2.40$ and $R = 1.77$ ($M = 0.94$). In these photographs, one can see large ring vortices, wavefronts of sound propagating upstream inside and outside the jet, and downstream-propagating wavefronts reflected from the nozzle-exit wall. The upstream-propagating waves excite the thin shear layer near the nozzle lip and produce periodic coherent structures. In Fig. 11 d, we can see a nascent ring vortex near the nozzle exit. This ring vortex is convected downstream and is enlarged with time (Figs. 11 d to 11 l and 11 a). When this enlarged ring vortex is convected some distance from the nozzle exit, another nascent ring vortex is produced near the nozzle exit (Fig. 11 j). This second smaller ring vortex is convected downstream faster than the first ring vortex, and finally the second ring vortex overtakes the first one to merge together (Figs. 11 k, 11 l and 11 a to 11 g). After the two vortices merged together, this coalesced vortex is convected with a nearly constant velocity and collides with the slender circular cylinder. By the interaction between the ring vortex and the cylinder, a new strong sound wave is emitted pulsatively (Figs. 11 a-b). In Figs. 11 b to 11 e, it is found that this wavefront propagates inside the jet. As is seen in Fig. 11 f, this wavefront splits into two parts. One part propagates inside the jet and the other propagates outside the jet.

It is important to emphasize that in our experiment two large collective coherent structures (two large ring vortices) merge together in a later stage of the feedback loop. This situation is clearly different from the suggestion by Ho and Nosseir.[1]

Although it was not confirmed in the present experiments, it can reasonably be considered that the two large coherent structures (ring vortices) are produced

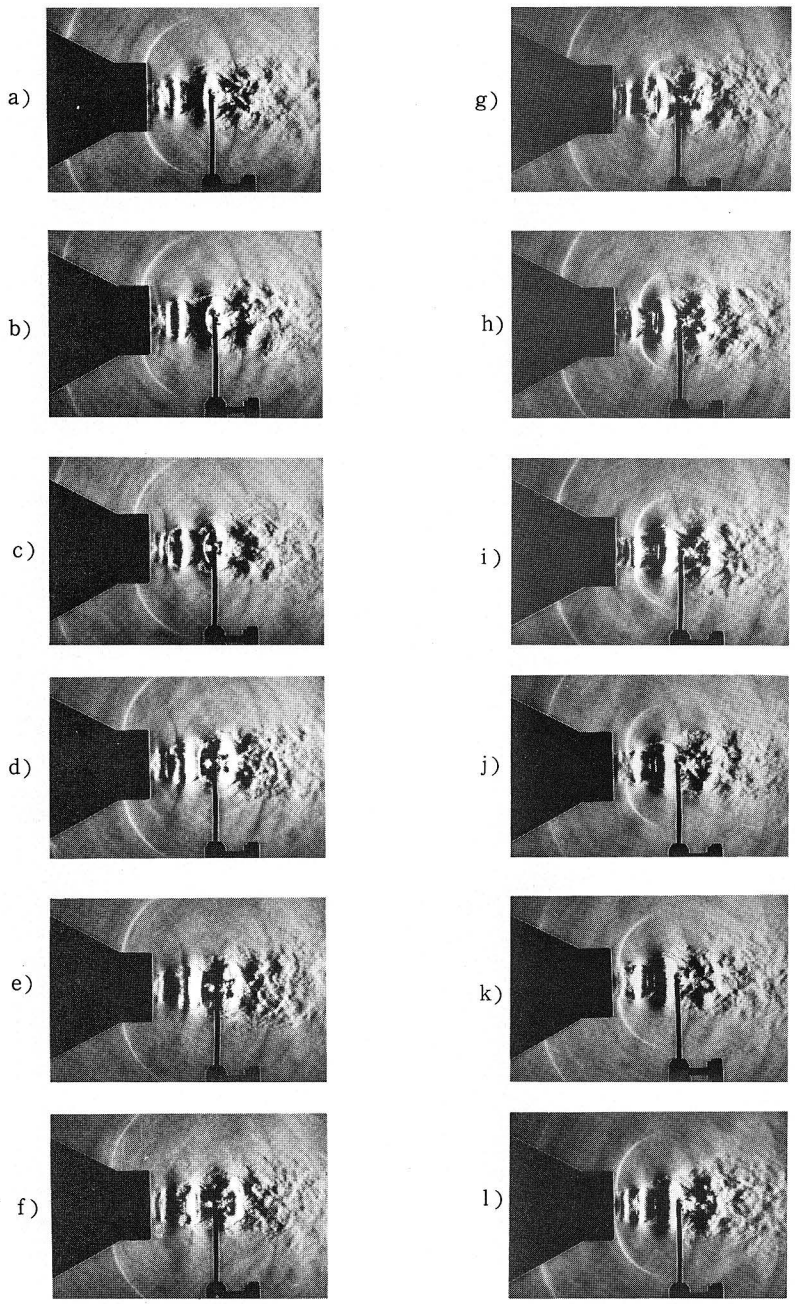

Fig. 11 Series of instantaneous photographs showing one cycle of impinging tone generation for $R=1.77$ ($M=0.94$) and $x/d=2.40$.

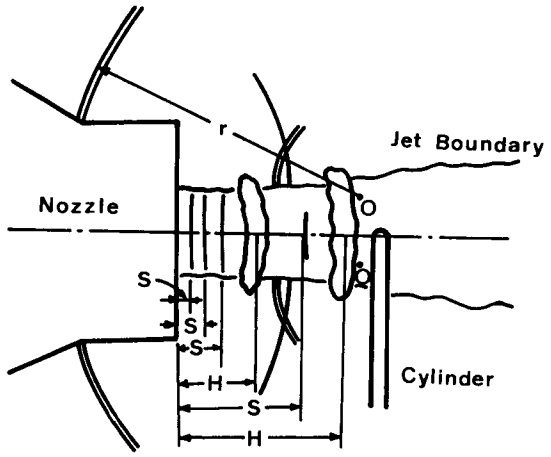

Fig. 12 Schema of the near-sound field when the cylinder is placed in the subsonic jet.

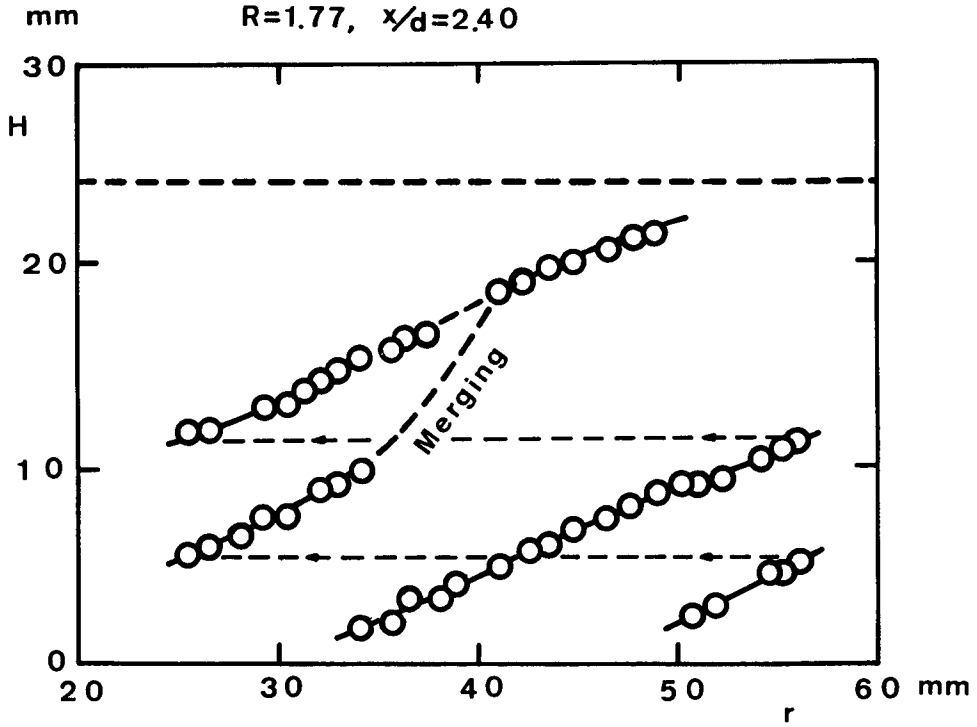

Fig. 13 Location of the ring vortex referred to the sound wavefront propagating through the ambient for $R=1.77$ and $x/d=2.40$.

near the nozzle exit under the influences of the sound waves propagating inside and outside the jet, respectively, during one cycle of the feedback loop.

In order to investigate the feedback loop more quantitatively, the distance r from the apparent sound source O to an upstream-propagating wavefront UW, and the distances H from the nozzle exit to the visual centers of the large ring vortices V along the jet axis were measured on a large number of instantaneous schlieren photographs. The notations are explained in Fig. 12 for a high subsonic jet. The measured data are shown in Fig. 13. Since the wave velocity outside the jet is nearly constant and equal to c_0, r/c_0 can be taken as a reference time. This result demonstrates surprisingly well the systematic and periodic behavior of the feedback loop. In this figure, $H = x$ is the location of the cylinder and $H = 0$ is that of nozzle exit. The interval between the left and right ends of the dotted line with arrows corresponds to the duration of one cycle of the feedback loop. The ring vortex is convected along the solid line. It can be seen from this figure that two large ring vortices are created during one cycle of the feedback loop, and the merging of the successive large ring vortices

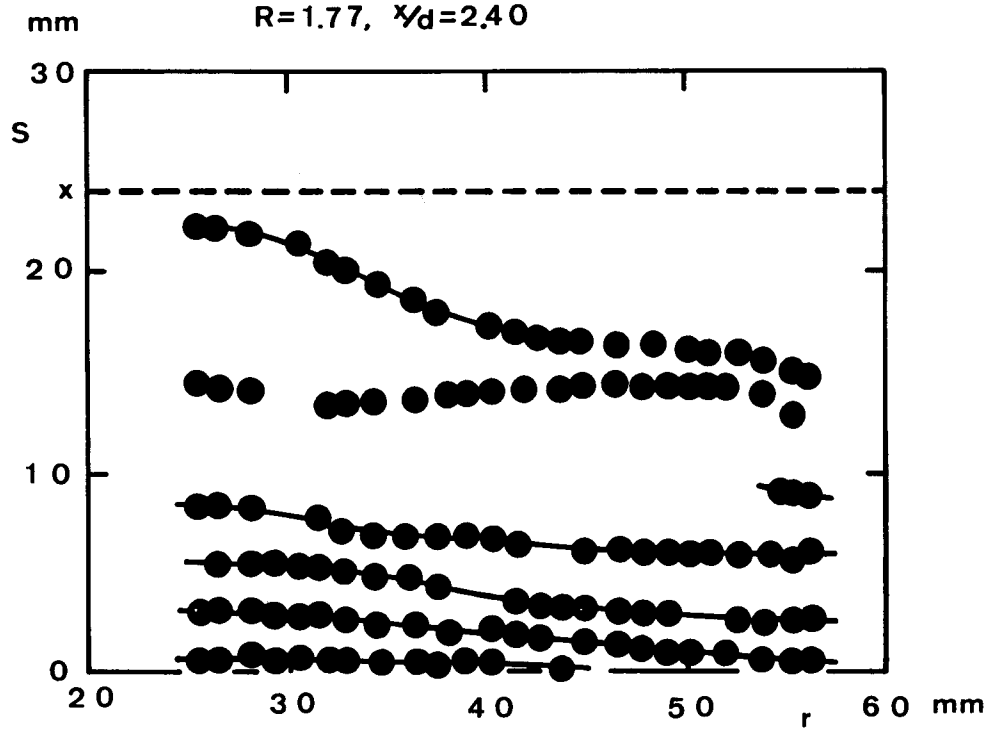

Fig. 14 Location of sound wavefront propagating inside the jet referred to the sound wavefront propagating through the ambient for $R = 1.77$ and $x/d = 2.40$.

has occurred. Since it was almost impossible to determine the location of each ring vortex during the merging of two successive ring vortices on the schlieren photographs, the loci of the two successive ring vortices are approximately estimated by the dotted lines during the merging in Fig. 13.

Figure 14 shows the relationship between the distances r and S, where S is the distance from the nozzle exit to the wavefront F propagating upstream inside the jet. In this figure, $S = x$ is location of the cylinder. The wavefronts inside the jet move along the solid lines. Several wavefronts are observed in the region between the nozzle exit and the cylinder. In the region near $S = 10$ mm, the wavefronts are concealed by the strong ring vortex and the locations of these wavefronts could not be determined by the schlieren photographs. The data for the wavefronts inside the jet near $S = 10$ mm are, therefore, not represented in Fig.14. It is proved in Fig. 14 that the strong sound waves surely propagate upstream inside the jet. This implies that the fringe pattern F appearing in the instantaneous photographs of the subsonic jets (Figs. 7 a and 7 c) is made of several upstream-propagating wavefronts inside the jet.

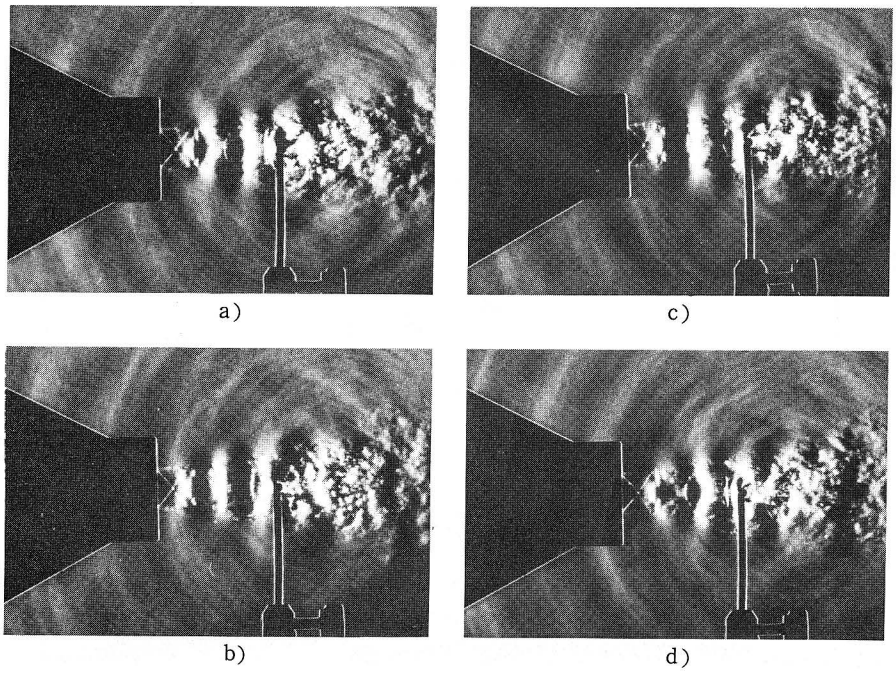

Fig. 15 Series of instantaneous photographs showing one cycle of impinging tone generation for $R = 2.45$ ($M = 1.21$) and $x/d = 3.00$.

B. Supersonic jet

Using the location of the upstream-propagating wavefront outside the jet as the reference time, we can demonstrate one cycle of the feedback loop of the impinging tone generation for $x/d = 3.00$ and $R = 2.45$ ($M = 1.21$) by a series of photographs, as shown in Figs. 15 a to 15 d. In these photographs, one can see large ring vortices, wavefronts of sound propagating upstream outside the jet, and a clear cellular structure. In this case, the nascent vortex grows rapidly when it passes through the rear edges of the cellular structures, and the merging phenomenon of the large successive ring vortices has not been observed. The distance r from the apparent sound source O to an upstream-propagating wavefront UW, and the distances H from the nozzle exit to the visual centers of the large ring vortices V along the jet axis were measured on a large number of instantaneous photographs. The measured data are shown in Fig. 16.

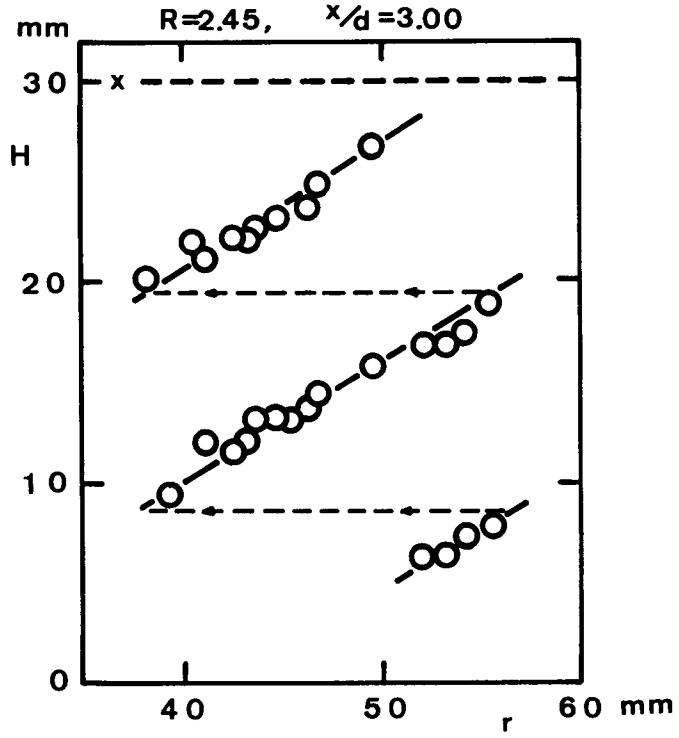

Fig. 16 Location of the ring vortex referred to the sound wavefront propagating through the ambient for $R = 2.45$ and $x/d = 3.00$.

In this figure, $H = x$ is the location of the cylinder. In this case, only one large ring vortex is produced during one cycle of the feedback loop, and the merging of successive large ring vortices has not occurred. This is consistent with the fact that the sound wave cannot propagate upstream in the supersonic flow inside the jet, and the ring vortex is created only by the excitation of the upstream-propagating sound wave outside the jet.

Since the gradients of the solid lines given in Figs. 13 and 16 represent the ratios of the velocities of the ring vortices to those of the sound waves propagating upstream outside the jet, the passage frequency of the ring vortices can be determined from these figures. It is reasonable to consider that the passage frequency of the ring vortices corresponds to the frequency of the discrete tone emitted from the jet. In Table 1, three frequencies f_V, f_{UW}, and f_M of a discrete tone are listed. The first frequencies f_V were determined based on the passage frequencies of the ring vortices shown in Figs. 13 and 16. The second frequencies f_{UW} were determined based on the wavelengths between two successive upstream-propagating wavefronts UW measured on the instantaneous photographs shown in Figs. 11 and 15. The last frequencies f_M were the microphone measurements shown in Figs. 3 and 4. Since the upstream-propagating wavefronts UW for the choked underexpanded jet shown in Fig. 15 are appreciably smeared, the frequencies f_V and f_{UW} determined from the photographs in Fig. 15 might contain errors of about 10%. Obviously, however, the agreement of these three frequencies is satisfactory both for the subsonic and the choked underexpanded jets.

Table 1 Frequency of impinging tone.

Frequency / Experimental Conditions	f_V (kHz)	f_{UW} (kHz)	f_M (kHz)
$R = 1.77$ $x/d = 2.40$	10.6	10.9	10.9
$R = 2.45$ $x/d = 3.00$	20.1	19.6	21.8

From these results, we can say that the impinging tones are emitted according to the following processes. First, the nascent ring vortices are generated near the nozzle exit under the influence of the sound propagating upstream. Second, in the subsonic jet, the jet shear layer grows rapidly due to the merging of two successive ring vortices. In the supersonic jet, the shear layer is grown by the interaction of the ring vortices with shock waves when they pass through

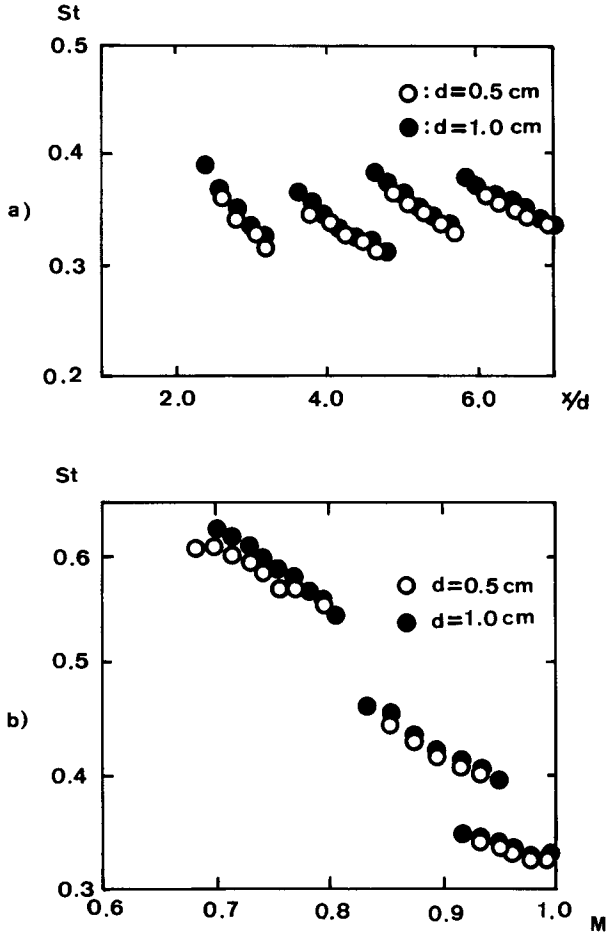

Fig. 17 Frequency characteristics of impinging tones for different nozzle diameters.

the regularly spaced shock wave system of the jet. Third, the impinging tones are emitted pulsatively from the jet due to the interaction of the large vortices with the cylinder. Finally, the strong wavefronts of these impinging tones propagate upstream and again excite the unstable thin layer of the jet near the nozzle exit to produce new nascent ring vortices. Such a process is repeated almost periodically.

C. Effect of nozzle diameter on frequency characteristics

When the nozzle diameter d was changed, and the other experimental condi-

tions (non-dimensional nozzle-to-cylinder distance x/d and flow Mach number M) were fixed, it was found that the frequencies of the discrete tones were inversely proportional to the nozzle diameter. Figure 17 a shows the relationship between the Strouhal number St and the non-dimensional nozzle-to-cylinder distance x/d for $M = 0.94$ and $d = 0.50$ cm and 1.00 cm nozzle diameters. The Strouhal number St is defined as $St = fd/U$. Figure 17 b shows the relationship between the Strouhal number St and the flow Mach number M for $x/d = 3.00$ and $d = 0.50$ cm and 1.00 cm. The agreement between these data for different nozzle diameters is good. This result is consistent with that obtained by Wagner[2] for the subsonic jet impinging on a flat plate placed normal to the jet axis.

6. Screech Tone

As was shown, for example, in Fig. 2 a, the screech tone is generated from a supersonic free jet. It will be important to compare the characteristics of the screech tone and the present impinging tone. Here, therefore, the screech tone is investigated.

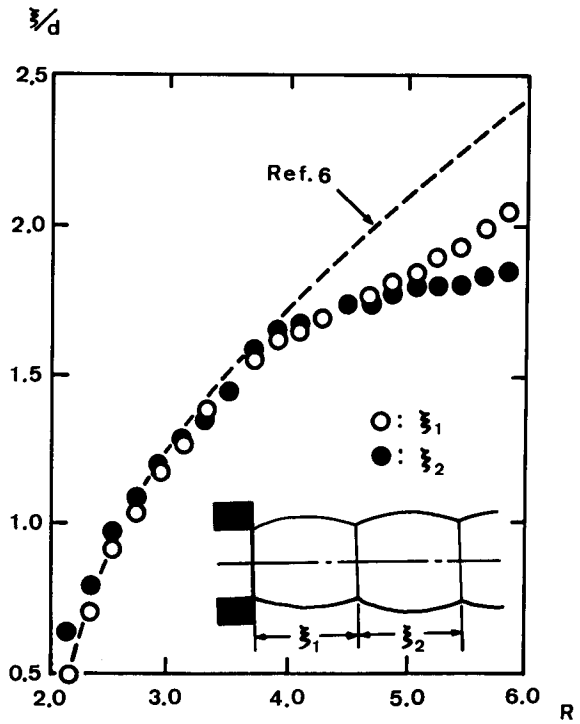

Fig. 18 Relationship between cell length and pressure ratio.

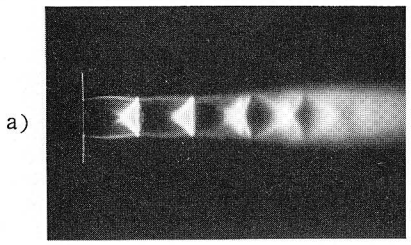

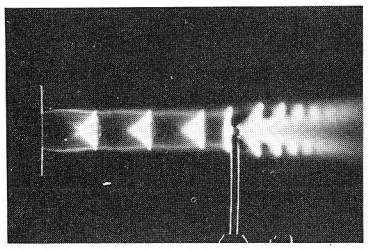

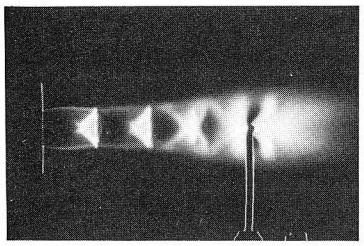

Fig. 19 Long-time-exposure photographs of jet for $R=3.90$: a) free jet, b) $x/d=5.40$, c) $x/d=5.80$.

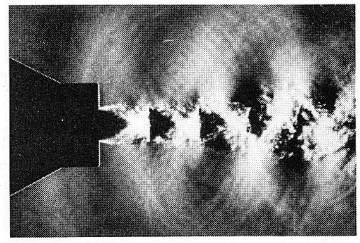

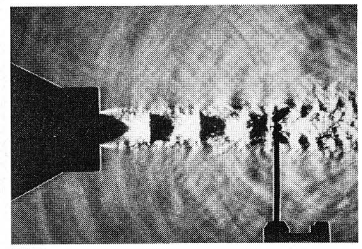

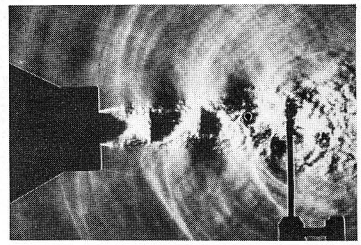

Fig. 20 Instantaneous photographs of jet for $R=3.90$: a) free jet, b) $x/d=5.40$, c) $x/d=5.80$.

For choked underexpanded jets, the lengths of the first two cells along the jet axis, ξ_1 and ξ_2, were measured by long-time-exposure photographs taken for the various pressure ratios R. The relationship between the cell lenghs ξ and the pressure ratio R is shown in Fig. 18. The frequency characteristics of the screech tone shown in Fig. 5 a are similar to those obtained by Powell.[6] Powell clarified the generation mechanism of the screech tone, and proposed that it is generated as the periodic eddy system traverses the regularly spaced shock wave system of the jet. Also, he proposed a rule for the frequency of the screech tone in the case of a circular nozzle by using empirical relation $\xi_1/d=1.2\sqrt{R-R_c}$ as follows:

$$f=(c_0/d)\,/\,3\sqrt{R-R_c} \qquad (6)$$

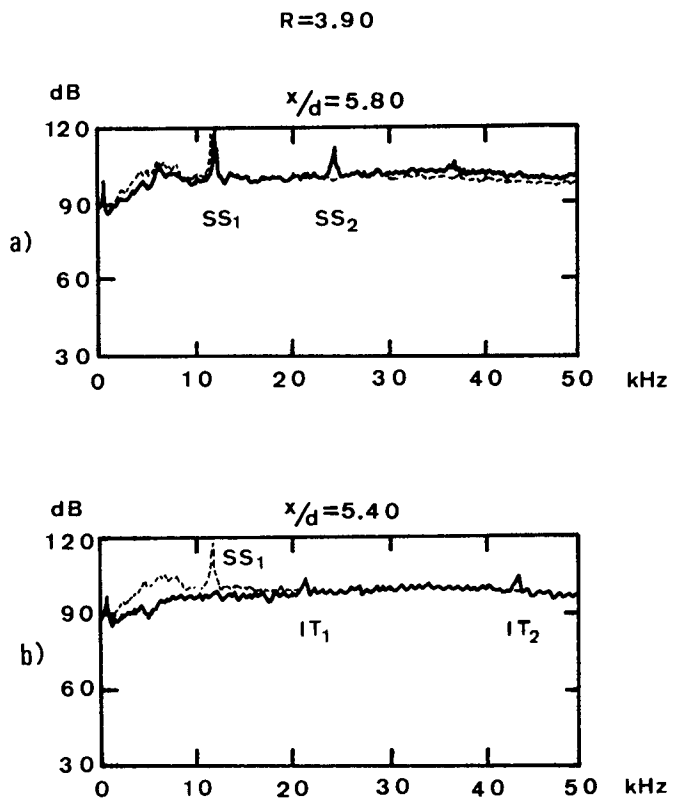

Fig. 21 Comparison of spectrum for free jet and that for jet with cylinder for $R=3.90$: a) $x/d=5.80$, b) $x/d=5.40$.

where R_c is the critical pressure ratio ($=1.893$) and c_0 is the speed of sound of the ambient.

The formula, Eq. (6), can be considered to be essentially equivalent to that proposed by Ho and Nosseir[1] for the impinging tone. If we assume that the sound sources are located on the rear edge of the first cellular structure, the time interval T for a feedback loop to close is given by

$$T=\xi_1/c_0+\xi_1/v \tag{7}$$

Further, assuming that the velocity of the downstream-convected coherent structure, v, is given by Eq. (3), one has the frequency of the screech tone by Eq. (5), where l is replaced by ξ_1. Substituting the relation $\xi_1/d=1.2\sqrt{R-R_c}$ into Eq. (4) yields a formula equivalent to Eq. (6).

With the experimental value of the cell length ξ_1 shown in Fig. 18, the frequency of the screech tone can be calculated from Eq. (5). The results for $n=1$ are shown in Fig. 5a by a solid line, and are compared with the acoustically measured data. The agreement of the experimental data and the theoretical predictions is good. This may support our hypothesis that the generation mechanism of the screech tone is essentially the same as that of the impinging tone proposed by Ho and Nosseir[1].

As was discussed, for instance, by Yu and Seiner[7], it is considered that helical mode of jet instability plays a direct role in the generation and maintenance of screech tone. In Figs. 19 and 20, a long-time-exposure and the corresponding instantaneous schlieren photographs of jets are shown for $R=3.90$. Figs. 19a and 20a are the free jet and Figs. 19b, 19c, 20b, and 20c are the jets with cylinders. The propagation of a strong asymmetric wave is well seen in Figs. 20a and 20c. The spectra of sounds emitted from the jets of Figs. 20a to 20c are shown in Fig. 21, where the dotted lines are for the free jet and the solid lines are for the jets with cylinders. The frequencies of the discrete tones *fuw* based on the wavelengths measured in Figs. 20a to 20c are *fuw*= 12, 13, and 23 kHz, respectively. These agree well with the microphone measurements shown in Figs. 21a and 21b. In the case of Figs. 20a and 20c, the jet oscillates upward and downward. This alternate deviation becomes larger with the axial distance, and is responsible for the emission of asymmetric sound waves, as is shown in these figures.

Since the frequency of the discrete tone for the jet in Fig. 20c almost coincides with that for the free jet in Fig. 20a, the discrete tone emitted from the former jet is obviously the screech tone. Then, in this case, placing the cylinder in the jet at $x/d=5.8$ results in an enhancement of the screech tone. On the other hand, the wavefronts shown in Fig. 20b (although relatively weak) are nearly symmetric, and the discrete tone is the impinging tone.

As has been discussed previously, the generation mechanism of the impinging tone is essentially the same as that of the screech tone. One of the key factors in the feedback loop is a phase matching. The frequency of the sound waves is determined by the passage frequency of a coherent structure through the cylinder or the rear edge of shock-cell structure. The upstream-propagating sound wave interferes with the very unstable shear layer near the nozzle exit. If this interference is in phase, then we have a strong resonance and an oscillatory flow. On the other hand, if the interference is out of phase, a quiet flow results.

When the cylinder is placed in a supersonic jet, we have two possible feedback loops. The characteristic lengths of these loops are the shock-cell

length and the distance from the nozzle exit to the cylinder, respectively. Under some favorable conditions, therefore, both loops may interact so as to enhance each other. Under some unfavorable conditions, an opposite case may also be expected, where these loops interact so as to suppress each other. The former case is realized in the jet shown in Fig. 20 b and the latter case is realized in the jet shown in Fig. 20 c. Since, however, the coherent structure may interact more strongly with the solid cylinder than with the shock wave, only a weak impinging tone is observed in the jet shown in Fig. 20 b.

7. Overall Sound Pressure Level

Figure 22 displays the overall sound pressure levels against the pressure ratio R for the nozzle-to-cylinder distances $x/d = 2.40$ and 3.00 ($d = 1.00$ cm). The overall sound pressure level becomes high for $R < 3.6$ by placing a cylinder in the jet. For $R > 3.6$, the situation is a little complicated. The overall sound pressure level for the jet with the cylinder becomes lower than that for the free jet for some particular locations.

In Fig. 23, the overall sound pressure levels are plotted against the nozzle-to-cylinder distance x/d for three different pressure ratios, $R = 1.77$, 2.45, and 3.90. For comparison, the overall sound pressure levels for the corresponding free jets are shown by dotted lines. As is shown in Fig. 23, the overall sound pressure levels change drastically in the range of $1.0 < x/d < 5.0$. The sharp and large changes of the sound pressure levels may be referred to the generation of strong impinging tones. The overall sound pressure levels for the free jets are 79.8, 93.0, and 101.8 dB for the pressure ratios $R = 1.77$, 2.45, and 3.90, respectively. For $R = 1.77$ and 2.45, the overall sound pressure levels radiated from the jets with cylinders are larger than those radiated from the corresponding free jets. However, for $R = 3.90$, the overall sound pressure level for the jet with a circular cylinder becomes higher or lower than that for the free jet, depending upon the location of the cylinder. This situation can well be understood by investigating the schlieren photographs shown in Figs. 19 and 20. Figure 19 a shows a long-time-exposure schlieren photograph of a choked underexpanded free jet for $R = 3.90$. In this figure, the first two cellular structures are very clear, but the cellular structrues downstream from them are smeared. This smearing of the downstream cellular structures indicates that the jet becomes remarkably unstable downstream from the second cellular structure, and the jet column undulates transversely.

Figures 19 b and 19 c show the long-time-exposure schlieren photographs of

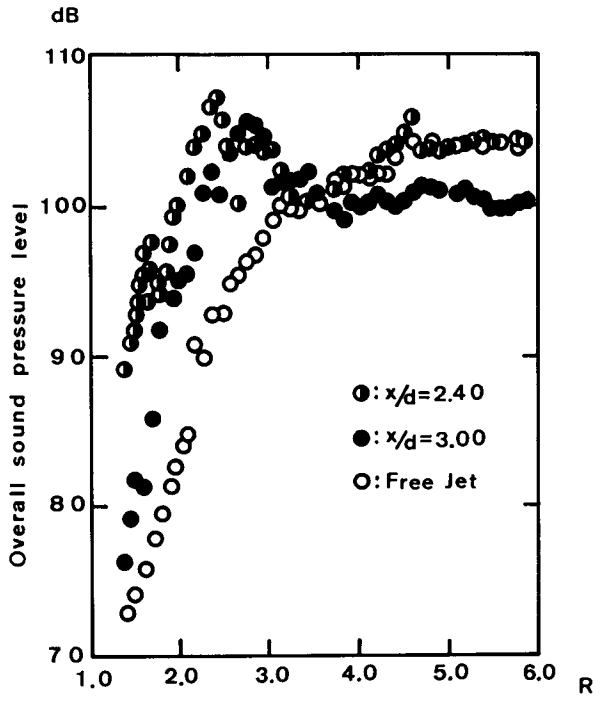

Fig. 22 Variation of overall sound pressure level when the pressure ratio is changed at fixed nozzle-to-cylinder distance.

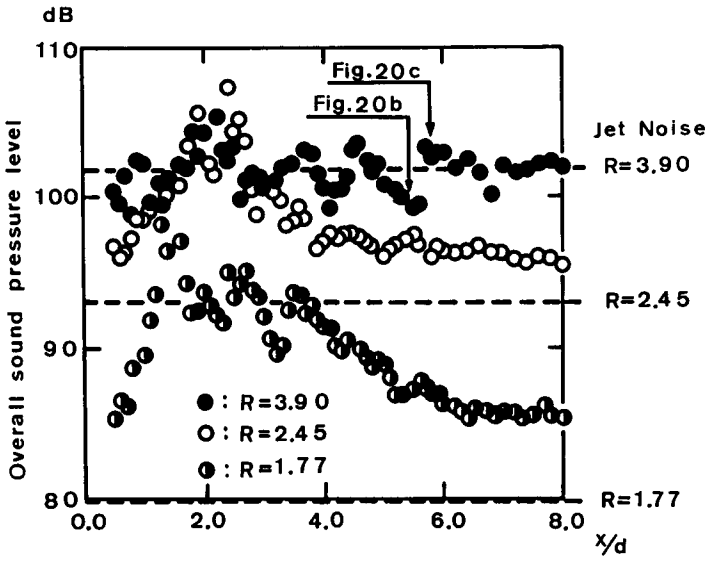

Fig. 23 Variation of overall sound pressure level when the nozzle-to-cylinder distance is changed at fixed pressure ratio.

jets with cylinders for the pressure ratio $R = 3.90$ and the nozzle-to-cylinder distances $x/d = 5.4$ and 5.8. It can be seen in Fig. 19 b that the cellular structures become sharper and clearer than those of the free jet. However, on the contrary, in Fig. 19 c, the cellular structures are smeared more than those of the free jet. Instantaneous schlieren photographs corresponding to the jets in Figs. 19 a to 19 c are shown in Figs. 20 a to 20 c, respectively. Obviously, the sound field outside the jet in Fig. 20 b is quieter, and that in Fig. 20 c is more noisy than that in Fig. 20 a. The overall sound pressure levels corresponding to the schlieren photographs of Figs. 20 b and 20 c are indicated on the curve in Fig. 23. The relationship between the jet instability and the overall sound pressure level can be well understood from this figure.

8. Discussions

In Ref. 2, Wagner made an experimental observation of the sound emitted from a high subsonic jet impinging on a flat plate placed normal to the jet axis, and on a slender body placed parallel to the jet axis inside the jet. He described that there is a strong resonance between an upstream-propagating sound wave and a downstream-convecting coherent structure produced by the upstream-propagating sound pressure near the nozzle lip. In his case, it was concluded that the sound wave prapagating upstream inside the jet plays an indispensable role for the resonance. Ho and Nosseir[1] made a similar experimental measurement of discrete tones generated from a high subsonic jet impinging on a flat plate placed normal to the jet axis. They also found a strong feedback loop resulting in an emission of strong discrete tones, and concluded that this feedback loop consists of a strong sound wave propagating upstream outside the jet and a downstream-convecting coherent structure produced by the sound pressure near the nozzle lip. Obviously, the two conclusions obtained in these two papers are contradictory to each other. In our experiment, the instantaneous photographs of high subsonic jets have shown that two major ring vortices (large and small ones) are produced during one cycle of the feedback loop. These two major ring vortices merge together before they impinge on the slender circular cylinder placed normal to the jet axis. It may be natural and reasonable to consider that these two major ring vortices are produced by the interaction of the thin shear layers near the nozzle lip and the pressure disturbances produced by the sound waves propagating upstream inside and outside the jet. At least for the present, we consider that both waves propagating inside and outside the jet play important roles for the construction of the present resonant

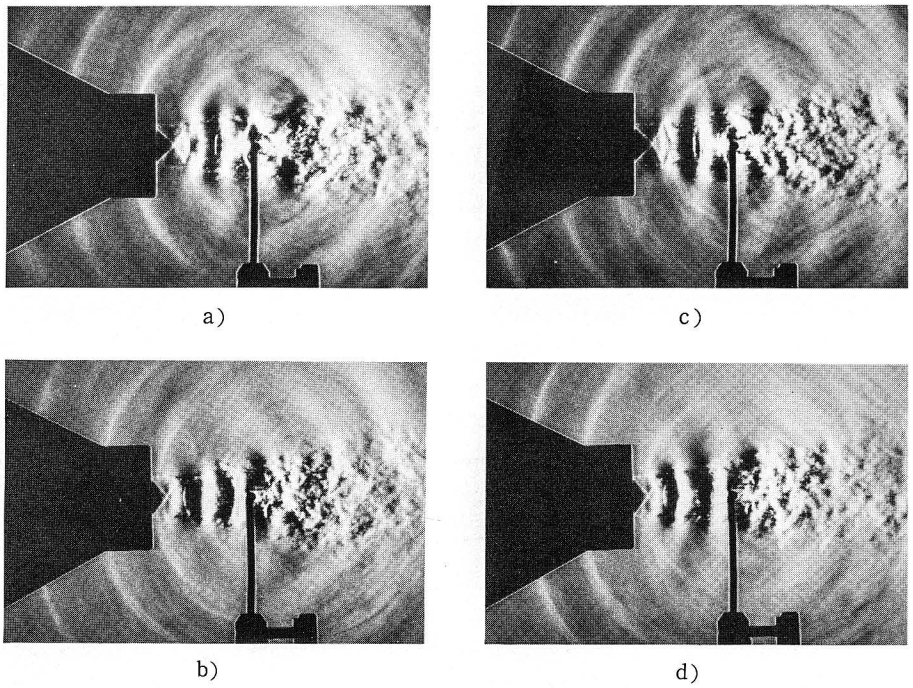

Fig. 24 Series of instantaneous photographs showing one cycle of impinging tone generation for $R=2.45$ and $x/d=2.40$.

feedback loop in the subsonic jet.

In the present study, however, the frequency of the impinging tone could be calculated by considering only a feedback loop consisting of one path outside the jet. This may suggest that the present impinging tone is almost completely controlled by the outside loop (in the subsonic jet). This does not, however, mean that the present result exculdes the possibility of existence of the inside loop. Perhaps, the outside loop might be much stronger than the inside loop and the former resonance overwhelms and suppresses the latter one.

In Ref. 6, Powell observed asymmetric wavefronts as well as symmetric ones for choked underexpanded jets. The asymmetric waves are also found in our experiment for the pressure ratio $R>3$. As will be seen, for example, in Figs. 20 a and 20 c, these asymmetric wavefronts have a spiral shape with the axis along the jet stream. Although such a spiral shape of wavefronts cannot be found clearly for the subsonic jet, there is no reason to exclude the possibility of emission of such a spiral mode of sound waves from the subsonic jet, when the cylinder is placed in the jet.

In Figs. 24 a to 24 d, a series of instantaneous schlieren photographs showing

one cycle of the feedback loop for the impinging tone are shown for $R=2.45$ and $x/d=2.40$. The sound spectrum for the jet is shown in Fig. 2 b. In this case, the period of one cycle of the feedback loop is not constant. Longer and shorter periods of feedback loops appear alternately, and then the wavelength between two successive wavefronts changes alternately. This situation is well reflected on the spectrum curve in Fig. 2 b. Such an alternate change of the period of the feedback loop might come from the strong interaction between the large ring vortices and the cellular structures. It must be emphasized that such an alternate change of the duration time of the feedback loop was an exceptional phenomenon observed in our present experiments.

The main flow structure of the supersonic jet can be divided into two parts. One is almost a regularly spaced shock-cell structure which is steady and stable itself. The other is an eddy system produced on the jet boundary due to the Kelvin–Helmholtz instability. The eddy system is essentially unsteady and interacts with the shocks to destabilize the shock–cell structure. If, therefore, the growth of the eddy system produced due to the Kelvin-Helmholtz instability is effectively suppressed by some external control, a jet structure with a relatively more stable shock-cell will result. In the present study, such a stable jet is realized, for example, in the jet shown in Fig, 20 b.

9. Conclusions

The objective of this work was to investigate the discrete tones gererated from high subsonic and choked underexpanded jets of air issuing from a circular nozzle and impinging on a slender circular cylinder placed normal to the jet axis. It was found that the impinging tone has the stepping frequency characteristics for a fixed cylinder location as the pressure ratio increases in both cases of high subsonic and supersonic jets. Also, it has a staging behaviour when the cylinder is moved along the jet axis for a fixed flow Mach number. It was shown that the discrete tones observed in our experiment were generated by a feedback loop similar to those proposed by Powell[6], and Ho and Nosseir.[1]

A series of instantaneous schlieren photographs of the flowfield showed the detailed process for the generation of the impinging tone as follows:

1) The impinging tone is emitted when the large-scale vortices impinge on the cylinder periodically.
2) A new nascent ring vortex is generated near the nozzle exit under the influence of the pressure of the discrete tone.
3) In the case of a high subsonic jet, the nascent ring vortex is convected

downstream faster than the ring vortex produced formerly, and these two successive ring vortices are merged into a large ring vortex. In the case of a supersonic jet, the nascent ring vortex is grown up when it passes through the regularly spaced shock wave system of the jet.

Further, the following interesting phenomena were found in our experiments:

1) The sound pressure level for the choked underexpanded jet is decreased by placing the cylinder at some locations in the jet for a particular jet Mach number.
2) The asymmetric waves are radiated for the pressure ratio greater than 3.

Acknowledgement

The authors would like to express their cordial thanks to Prof. T. Sakurai for his valuable discussions about the feedback loop, and to Profs. T. Matsuda and J. Katsura for their kind criticism.

References

1) C. M. Ho and N. S. Nosseir; J. Fluid Mech. **105**, 119 (1981).
2) R. F. Wagner; Z. Flugwiss. **19**, 30 (1971).
3) H. A. Marsh; J. Acoust. Soc. America **33**, 1065 (1961).
4) A. Krothapalli; AIAA J. **23**, 1910 (1985).
5) Y. Umeda, H. Maeda, and R. Ishii; AIAA J. **24**, 693 (1986).
6) A. Powell; Proc. Phys. Soc. London, B, **66**, 1039 (1953).
7) J. C. Yu and J. M. Seiner; AIAA paper, 83-0706 (1983).